Crystal field and magnetocrystalline anisotropy in ErNiAl

P. Javorský* and M. Diviš
Department of Electron Structures, Charles University, Ke Karlovu 5, 121 16 Prague 2, The Czech Republic

H. Sugawara and H. Sato
Faculty of Science, Metropolitan University, Minami-Ohsawa 1-1, Hachioji-shi 192-0397, Japan

H. Mutka
Institut Max von Laue Paul Langevin, rue Jules Horowitz, 38042 Grenoble Cedex 9, France
(Received 23 January 2001; revised manuscript received 29 May 2001; published 29 November 2001)

We present a study of the crystal field and electronic structure in an ErNiAl intermetallic compound based on the inelastic neutron spectroscopy, magnetic susceptibility, specific heat data, and first-principles density-functional calculations. We have fully determined the lower half of the ground-state multiplet energy-level scheme in ErNiAl. Several possible sets of the crystal-field parameters have been found to describe all our experimental data. Magnetic-susceptibility data revealed a rather weak magnetocrystalline anisotropy.

DOI: 10.1103/PhysRevB.65.014404 PACS number(s): 75.30.Cr, 75.40.Cx, 61.12.−q

I. INTRODUCTION

ErNiAl belongs to a large group of RTX compounds (R, rare earth; T, transition metal; X,p metal) crystallizing in a hexagonal ZrNiAl-type structure (space group $P\bar{6}2m$). The structure is a layered one, with R-T and T-X planes alternating along the hexagonal c axis. Both layers are shown in Fig. 1. The rare-earth atoms are located in the $3(g)$ positions $(x,0,1/2)$, $(0,x,1/2)$, and $(\bar{x},\bar{x},1/2)$ with $x=0.596(2)$ for ErNiAl as determined from neutron diffraction.[1] The point symmetry at R sites is orthorhombic ($m2m$). Within this group of RTX compounds, RNiAl have been studied most intensively. Magnetic structures in these compounds are rather complex,[2–4] with the rare-earth magnetic moments often much lower than R^{3+} free-ion values. This behavior was ascribed to the crystal-field (CF) interaction. The CF certainly plays an important role in determining the magnetocrystalline anisotropy. In some systems, a knowledge of the lowest-order term in the CF Hamiltonian is sufficient to determine the anisotropy. This is not the case in the aforementioned RTX series. The determined easy-magnetization axes in many of these compounds[5,6] indicate that higher-order CF terms also have to be taken into account in these compounds. A good knowledge of CF parameters is of high importance for further studies of this system. Until now, only very scarce information has been available concerning the crystal field in the whole family of RTX compounds.[7–9]

ErNiAl orders magnetically below $T_N=6.2$ K.[1] As inferred from neutron diffraction, erbium magnetic moments form, in a zero magnetic field, a noncollinear antiferromagnetic structure within the basal plane. The orthorhombic CF splits the $^4I_{15/2}$ ground state multiplet of Er^{3+} into eight doublet energy levels. Our previous inelastic-neutron-scattering (INS) experiment[7] revealed the existence of two excited CF levels at 2.1 and 6.7 meV. The existence of an energy level at ≈ 1 meV was deduced from specific-heat data.[7] The relatively poor statistics of this INS experiment did not allow us to make any final conclusions about the CF-level scheme in ErNiAl. Here we present a more detailed study based on an INS data set, single-crystal susceptibility, and specific heat. These experimental results are compared with results of first principles electronic structure calculations based on a density functional (DFT) theory.

II. EXPERIMENT

The ErNiAl single crystal was grown by the Czochralsky method in a tetra-arc furnace from a stoichiometric melt of constituent elements (purity $4N$ for Er, $5N$ for Ni, and $6N$ for Al). The final single-grain crystal had a cylindrical shape with a diameter of 2 mm and a length of 7 mm. The polycrystalline sample (≈ 15 g) used for the powder neutron scattering experiment was prepared in a cooled copper crucible using high-frequency heating. The x-ray analysis

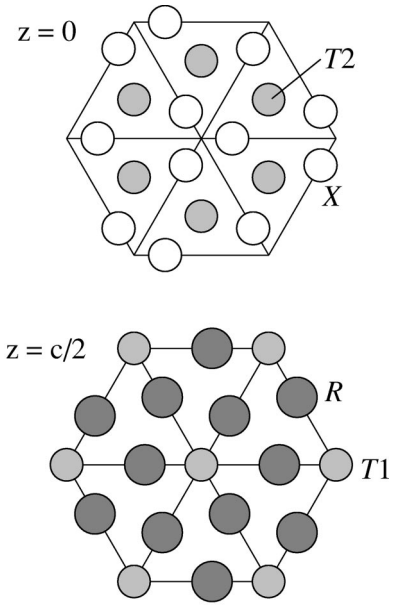

FIG. 1. Schematic picture of the two basal-plane layers of the ZrNiAl-type crystal structure.

showed the sample to be a single phase. The determined lattice parameters $a=(6.972\pm0.002)$ Å and $c=(3.799\pm0.001)$ Å are in a good agreement with the values determined in the former study.[1]

The inelastic neutron spectra were taken at several temperatures between 2 and 100 K on the IN5 time-of-flight spectrometer in the ILL Grenoble, with three different incident wavelengths: $\lambda=5.0$ Å ($E_i=3.3$ meV), $\lambda=3.8$ Å ($E_i=5.7$ meV), and $\lambda=2.5$ Å ($E_i=13.1$ meV). In order to minimize the contribution of phonon scattering, which increases quadratically with the scattering angle, only the low-angle detectors were summed up. Data measured on an empty sample container were subtracted from all the spectra, and the relative efficiencies of the detectors were calibrated by measurement on a standard vanadium sample.

The magnetic susceptibility was measured using a superconducting quantum interference device magnetometer (Quantum Design, installed at the Institute of Physics, Czech Academy of Sciences, Prague) in a temperature range 6–300 K on a sample (25 mg) cut from the crystal. The specific heat was measured by a relaxation technique (sample mass 14 mg) using the PPMS-14 system (Quantum Design, installed in the Joint Laboratory for Magnetic Studies in Prague).

III. THEORETICAL ASPECTS

The interaction with the crystal field, produced by the neighboring core charges and the valence electronic charge density, is the strongest perturbation of the free-ion $4f$ shell state of trivalent rare-earth ions in ErNiAl. As the Er^{3+} ions are located on sites with an orthorhombic symmetry, the interaction Hamiltonian can be written as.[10]

$$H_{CF}=B_2^0O_2^0+B_2^2O_2^2+B_4^0O_4^0+B_4^2O_4^2+B_4^4O_4^4 + B_6^0O_6^0+B_6^2O_6^2+B_6^4O_6^4+B_6^6O_6^6, \quad (1)$$

where B_n^m are the so-called crystal-field parameters and O_n^m are the operator equivalents. To search for the crystal-field parameters systematically , this crystal-field Hamiltonian can be also transformed into a more appropriate form:[11]

$$H_{CF}=W\sum_{n,m} x_{n,m}\hat{O}_n^m, \quad \sum_{n,m}|x_{n,m}|\leqslant 1. \quad (2)$$

The transformation between the parameters $x_{n,m}$ and the B_n^m parameters was given in Ref. 11. For the orthorhombic symmetry, there are eight $x_{n,m}$ parameters, $x_{n,m}\in\langle -1;1\rangle$ as follows from Eq. (1), and the energy scale W.

The values of the B_n^m parameters are determined by combining different approaches. In regular Er^{3+} sites we calculate the unknown parameters B_n^m by numerically solving the *inverse secular problem*, where the experimental CF energy levels are considered to be the eigenvalues of the secular equation of H_{CF}.

To obtain an independent estimate of B_2^0, we use an *ab initio* method recently applied to rare-earth intermetallics[12] and cuprates.[13] Within this method the electronic structure and related distribution of the ground-state charge density in the studied compounds are obtained from the first-principles calculations based on the density-functional theory. Exchange and correlation effects are treated within the local-spin-density approximation (LSDA) and the general gradient approximation (GGA).[14] Scalar relativistic Kohn-Sham equations are used to obtain the self-consistent single-electron wave functions. The calculations described in Sec. IV were performed using the full potential linearized augmented plane-wave method (LAPW) implemented in the latest version (WIEN97) of the original WIEN code.[15] Atomic sphere radii of $R_{\mathrm{MT}}=2.8$, 2.0, and 1.5 a.u. (MT is muffin tin) were taken for R=Er or Lu, Ni, and Al, respectively. The basis functions were represented by 1500 plane waves (more than 100 APW/atom) plus local orbitals of Er or Lu $(5s,5p)$, Ni$(3p)$, and Al $(2p)$ semicore states, which lie less than 82 eV below the Fermi level. The local orbitals avoid the problem of nonorthogonality, that can occur in calculations in which the semicore states are either frozen or treated in a separate energy window. A maximum of $l=12$ was adopted for the expansion of the radial wave function. Inside the spheres the crystal potential and charge density were expanded into crystal harmonics up to the sixth order. For the Brillouin-zone integrations a tetrahedron method[15] with 36–105 special k points was used.

The Er $4f$ states in the spherical part of the potential are treated as atomiclike core states (open-core treatment).[16] Er in the studied compound is characterized by the integer occupation number $N_{4f}=11$. A similar approach was successfully used, e.g., in the DFT calculations for $PrBa_2Cu_3O_6$.[17] For the sake of comparison we also performed DFT calculations for LuNiAl. In this case the $4f$ valence states are fully occupied, and we treated them in two separate calculations as ''normal'' valence $4f$ states or ''open core'' $4f$ states.

Within the DFT the parameter B_2^0 of the CF Hamiltonian, originating from the effective potential V inside the crystal, can be written as

$$B_2^0=a_2^0\int_0^\infty |R_{4f}(r)|^2V_2^0(r)r^2dr. \quad (3)$$

The nonspherical component $V_2^0(r)$ reflects, in addition to nuclear potentials and the Hartree part of the interelectronic interaction, the exchange correlation term which accounts for many-particle effects. The radial wave function R_{4f} describes the radial shape of the localized $4f$ charge density of an Er^{3+} ion in the studied compound. It is well known that the use of self-consistent ''open core'' R_4f leads to a poor description of the CF interaction. The reason for this is that the so-called ''self-interaction'' potential ''felt'' by a localized $4f$ electron is not correctly treated within the LSDA.[16] Therefore, the present study uses the value of R_4f in Eq. (3), resulting from the self-interaction-corrected LSDA atomic calculations with occupation numbers of the valence electrons of Er $(6s,5d,6p)$ fixed to their values obtained in the self-consistent LSDA calculations in a given Er compound. This approach[18] was found to give a $4f$ charge density, very close to that obtained from more rigorous DFT band calculations including self-interaction corrections for the $4f$ states directly.[16]

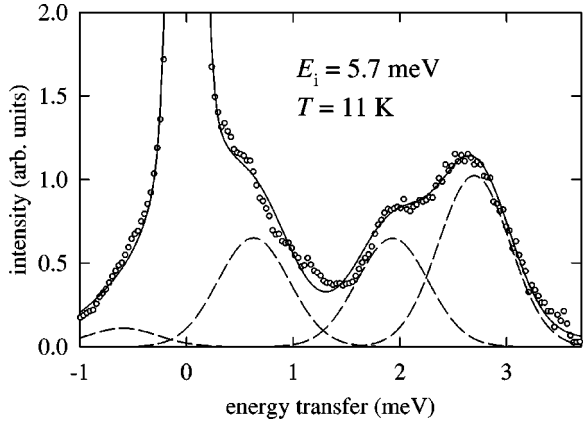

FIG. 2. Inelastic spectra of ErNiAl for $E_i = 5.7$ meV at 11 K after all the corrections. The dashed lines represent the individual peaks, the full line is their sum.

To calculate $V_2^0(r)$ we rewrite the right-hand side of Eq. (3) as a sum of two contributions,

$$B_2^0 = a_2^0 \left(\int_0^{R_{\mathrm{MT}}} |R_{4f}(r)|^2 U_2^0(r) r^2 dr + \int_{R_{\mathrm{MT}}}^{\infty} |R_{4f}(r)|^2 W_2^0(r) r^2 dr \right), \quad (4)$$

where $U_2^0(r)$ and $W_2^0(r)$ are, respectively, the components of the effective potential inside the atomic sphere with radius R_{MT} and in the interstitial region. The term $U_2^0(r)$ is readily obtained with the WIEN97 code. The new feature of our approach is that $W_2^0(r)$ is calculated using the exact transformation of the interstitial plane-wave representation of the potential into the spherical Bessel functions. The conversion factor $a_2^0 = \sqrt{5/16\pi}$ establishes the relation between the LAPW symmetrized spherical harmonic and the real tesseral harmonics that transform in the same way as tensor operator O_2^0 in Eq. (1).

Both the calculated CF parameters and the parameters found by analyzing experimental data have been obtained using the same coordinate system. The B_2^0 parameter is related to the axis aligned with the hexagonal c axis. The z axis is also defined as a hexagonal axis when calculating the magnetic susceptibility.

IV. RESULTS AND DISCUSSION

Three peaks are seen in the ErNiAl neutron spectra measured for $E_i = 5.7$ meV (shown in Figs. 2 and 3). They all are rather broad with a full width at half maximum approximately equal to 0.8 meV. The first (at ≈ 0.7 meV), seen as an asymmetric broadening of the central elastic peak and the third one (at 2.70 meV) can be described as the crystal-field transitions from the ground state (E_0) to the first two excited levels (E_1 and E_2). The middle peak is at 1.95 meV, that is, close to the difference between these two levels. It can be understood as an $E_1 \rightarrow E_2$ transition. Such an interpretation is corroborated by intensity variations of the observed peaks

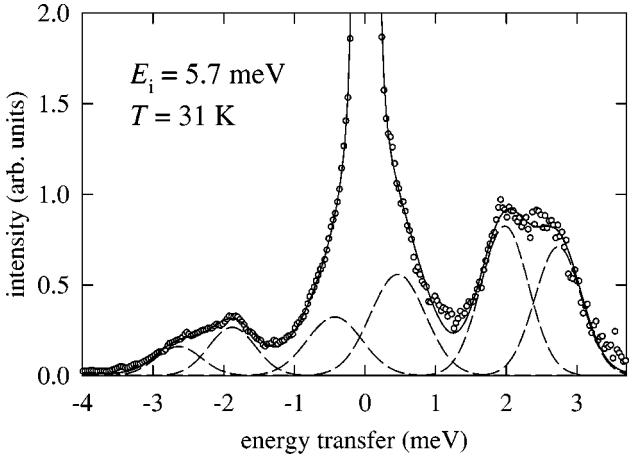

FIG. 3. Inelastic spectra of ErNiAl for for $E_i = 5.7$ meV at 31 K after all the corrections. The dashed lines represent the individual peaks; the full line is their sum.

with temperature: $I(E_1 \rightarrow E_2)$ increases with increasing temperature because the E_1 state becomes more populated. Furthermore, such a level scheme does not contradict the specific-heat data, as we show below. The position of the first excited level can then be determined more precisely from the $E_1 \rightarrow E_2$ transition than from the $E_0 \rightarrow E_1$ transition. The shape of the first two peaks is not fitted well at 11 K. The possible reason for this could be the dispersive character of the first excited level due to exchange interactions.

The spectra measured for $E_i = 13.1$ meV are shown in Figs. 4 and 5. Here we observe an additional peak around 6.5 meV that we attribute to the $E_0 \rightarrow E_3$ and $E_1 \rightarrow E_3$ transitions. Thus it is a sum of two peaks, separated by $(E_1 - E_0)$. We cannot also exclude the existence of a further level around this energy. The $E_0 \rightarrow E_4$ and $E_1 \rightarrow E_4$ transitions would then also contribute to this observed peak. Comparing the 11- and 31-K spectra, we see a clear increase of the intensity of a peak having a maximum at 4.3 meV. The temperature development of its intensity suggests that it is due to the $E_2 \rightarrow E_3$ transition. Its position can then be used as the most precise tool for a determination of the third excited level.

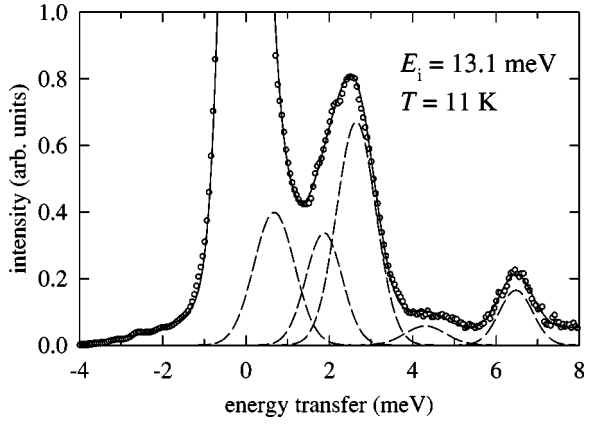

FIG. 4. Inelastic spectra of ErNiAl for for $E_i = 13.1$ meV at 11 K after all the corrections. The dashed lines represent the individual peaks; the full line is their sum.

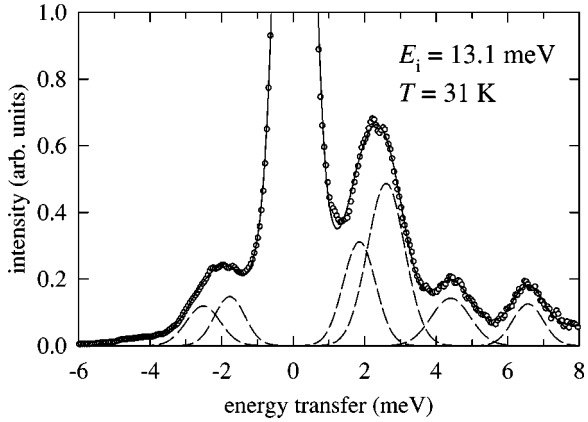

FIG. 5. Inelastic spectra of ErNiAl for for $E_i = 13.1$ meV at 31 K after all the corrections. The dashed lines represent the individual peaks; the full line is their sum.

There are no substantial changes in the spectrum measured at 100 K (not shown).

The spectra measured with $E_i = 3.3$ meV (up to 1.5 meV in the energy-loss part) show just a broadening of the elastic peak due to the $E_0 \rightarrow E_1$ transition. Its width does not decrease considerably compared to data for $E_i = 5.7$ meV. Therefore, they cannot be used to obtain a more precise determination of the E_1 level, and have not been shown here.

The location of the first three excited CF levels, as derived from all the neutron spectra, can be summarized as follows: $E_1 = (0.75 \pm 0.10)$ meV, $E_2 = (2.70 \pm 0.05)$ meV, and $E_3 = (6.9 \pm 0.2)$ meV. Such an energy-level scheme is in agreement with the observed intensities of the peaks in the energy-gain and energy-loss parts of the spectra measured at different temperatures considering gradual population of excited states with temperature.

Compared to the former INS data,[7] the overall picture is the same, but with small shifts in the energy levels. The statistics and resolution of the present experiment is, however, considerably higher, and allows to see two transitions in the peak around ≈ 2.1 meV. Furthermore, the existence of the first excited level below 1 meV, previously deduced from $C_p(T)$ data,[7] has been confirmed.

The inverse magnetic susceptibility of ErNiAl, measured with the magnetic field applied parallel or perpendicular to the c axis, is shown in Fig. 6. The measurements with field applied along different basal-plane directions give almost identical results. All these data reveal a negligible magnetic anisotropy within the basal plane and a very weak anisotropy between the c-axis and the basal plane. The weak anisotropy in ErNiAl is in contrast with the huge magnetocrystalline anisotropy in the isostructural UTX compounds.[19] Relatively weak anisotropy seems to be a more general behavior of these RTX compounds.[20,8] Of course, the origin of the anisotropy in the UTX compounds is different. While the CF is responsible for the anisotropy in these rare-earth materials, hybridization effects between the uranium $5f$ states and the ligand states plays a crucial role in the isostructural UTX compounds.

Let us now turn to the specific-heat data. To determine the magnetic heat capacity, one first has to subtract the nonmagnetic part, which in general consists of electronic and phonon contributions. To determine these contributions, we have measured the $C_p(T)$ of an isostructural LuNiAl. The γ-coefficient of the electronic specific heat has been determined from the low-temperature part of the C_p/T vs T^2 plot (see the inset in Fig. 7) as 8.4 mJ mol^{-1}K^{-2}. For the phonon part, we assumed the following approximation: the total phonon spectrum consists of three acoustic branches that we describe by a Debye model and characterize by one Debye temperature θ_D, and six optical branches, described by an Einstein model and characterized by two Einstein temperatures θ_E, each describing three branches. To account for the anharmonicity effects, we have used the expression derived by Martín.[21] For simplicity, we assume the anharmonicity coefficients C_j to be same for all phonon branches,

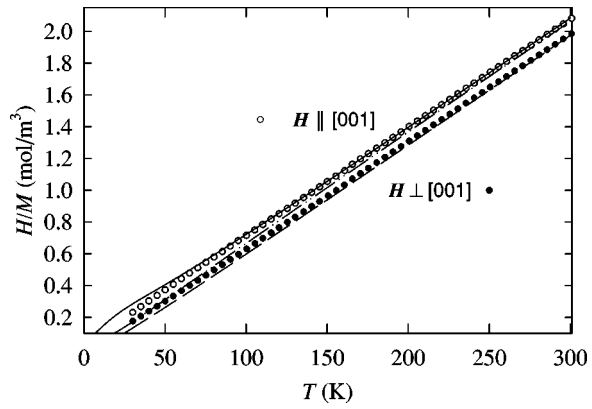

FIG. 6. Temperature dependence of the inverse magnetic susceptibility of ErNiAl. Experimental data obtained with a field of 1 T parallel and perpendicular to the c axis are shown; applying the field along different basal-plane directions gives, within experimental errors, the same results. The lines represent an illustrative example of calculated $H/M(T)$ dependencies for $H \| [001]$ (full line), $H \| [100]$ (dashed line), and $H \| [1-20]$ (dash-dotted line) using a set of CF parameters considered as acceptable (data for set No. 12 in Table I).

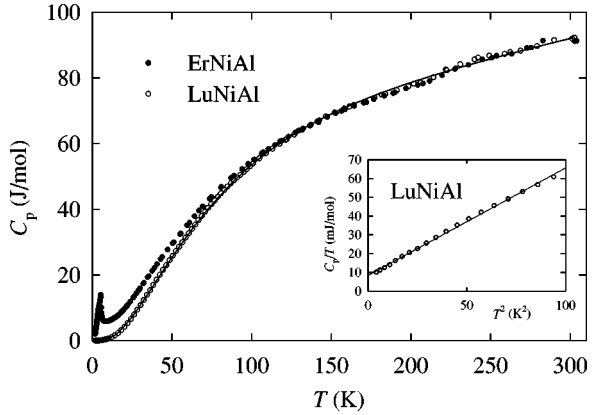

FIG. 7. Temperature dependence of the specific heat of ErNiAl and LuNiAl. The line represent the fit to $C_{\rm el} + C_{\rm ph}$ with $\gamma = 8.4$ mJ mol^{-1}K^{-2}, $\theta_D = 150$ K, $\theta_{E1} = 213$ K, $\theta_{E2} = 360$ K, $C_D = C_{E1} = C_{E2} = 7 \times 10^{-4}$ K^{-1}.

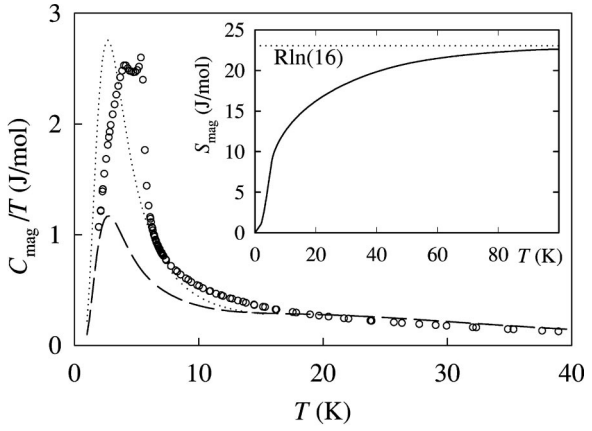

FIG. 8. Magnetic contribution to the specific heat of ErNiAl; the dashed line represents the Schottky (CF) contribution obtained for CF doublets at 0, 0.75, 2.7, and 6.9 meV, and four further doublets above 6.9 meV (above 80 K); the dotted line represents the specific heat obtained for the same level scheme assuming additional splitting of the doublet ground state into two singlet levels separated by 1.1 meV.

$$C_{\mathrm{ph}} = N_A k_B \sum_j \frac{1}{1-C_j T} \frac{x_j^2 e^x}{[\exp(x_j)-1]^2} + \frac{9}{1-C_D T} \frac{T^3}{\theta_D^3} \int_0^{\theta_D/T} \frac{x^4 e^x}{(e^x-1)^2} \, dx, \qquad (5)$$

where N_A is the Avogadro constant, k_B is the Boltzmann constant, and $x_j = \theta_{Ej}/T$. The best agreement with the measured data is obtained for the following parameters: $\theta_D = 150$ K, $\theta_{E1} = 213$ K, $\theta_{E2} = 360$ K, and $C_D = C_{E1} = C_{E2} = 7 \times 10^{-4}$ K^{-1}. We have also taken these values to describe the nonmagnetic specific heat of ErNiAl, that should be a good approximation because the molar mass and volume of LuNiAl and ErNiAl are quite close to each other. We should note that any simpler model of the phonon specific heat (e.g., a single Debye temperature describing all the phonon branches or excluding the anharmonicity effects) fails to describe the observed LuNiAl data.

The comparison of ErNiAl data and the approximation for the nonmagnetic part shows that the main difference occurs below 100 K. Above $\approx$100 K, the ErNiAl and LuNiAl data are almost identical. The ErNiAl magnetic entropy (see the inset in Fig. 8) reaches a value of 22.5 J/mol K at $T = 90$ K, very close (98%) to R ln(16) = 23.05 J/mol K expected for Er^{3+} ions, and remains then almost constant up to 300 K.

The dashed line in Fig. 8 shows the magnetic (Schottky) contribution due to the population of CF levels, assuming the level scheme derived from our INS data. The difference between this curve and the measured data gives a magnetic entropy of 6.6 J/mol K$\cong$1.15 R ln(2) at $T = 20$ K. As expected, it confirms the doublet ground state. The doublet ground state splits at low temperatures due to an internal magnetic field caused by the ordered erbium magnetic moments. This splitting was observed as an additional peak at 1.1 meV in the INS spectrum of ErNiAl at 4 K (i.e., in the magnetically ordered state).[7] In a very simplified model, the doublet ground state splits into two singlet energy levels without any dispersion. Taking the value of 1.1 meV as an estimation of this splitting, we obtain the specific heat represented by the dotted line in Fig. 8. It is in a good qualitative agreement with the measured data. Of course, the magnetic excitations have a complex character, and the $C_p/T(T)$ data below and around the ordering temperature of 6.2 K cannot be fully described in such a simple model.

We tried to find a set of CF parameters giving a reasonable agreement with all our experimental data. All the $x_{n,m}$ parameters have been scanned from -1 to 1 with a step of 0.05 without any preliminary assumptions. First we have selected such $x_{n,m}$ sets leading to the first three excited levels within the accuracy of their determination as given above, and to relative intensities of transitions between these levels which are in a satisfactory agreement with the experimental ones. The energy scale W has been fixed to account for the energy splitting determined with the highest relative precision: $E_2 = 2.70$ meV. Compared to the former INS experiment,[7] the energy splitting between the levels and intensities has been determined with considerably smaller error, that substantially reduces the number of solutions.

The obtained sets of $x_{n,m}$, have then been used to calculate the inverse magnetic susceptibility, and were compared with the experimental data. To account for the effect of the exchange coupling, we have used a simple mean-field approximation[22]

$$\frac{1}{\chi} = \frac{1}{\chi_{\mathrm{CF}}} - \Lambda, \qquad (6)$$

where Λ is a molecular field constant, and $\Lambda = 0.30\mathrm{T}/\mu_B$ in the case of ErNiAl with $T_c = 6.2$ K. The majority of the tested sets was ruled out in this way, e.g., all sets resulting in a negative B_2^0 parameter can be excluded. As an example, the $H/M(T)$ curves, calculated using one of the sets considered to be in satisfactory agreement with the experiment, are shown in Fig. 6. In distinction from experiment, it shows a certain anisotropy within the basal plane. An effect of comparable size can be obtained by small variations of the CF parameters, comparable with our searching grid. Therefore, in order to miss no possible solution, we do not rule out the sets of CF parameters which give similar discrepancy to the experimental data.

Finally, the remaining sets of CF parameters were compared with the measured $C_p(T)$ data. Below $\approx$40 K, the calculated Schottky specific heat agrees with the experimental data (see Fig. 8) in all cases, as it depends mainly on the first excited levels already determined by the INS analysis. Additional information is thus obtained from the temperature region above $\approx$50 K. All $x_{n,m}$ sets that lead to a large energy splitting above $E_3 = 6.9$ meV (80 K), and thus to a relatively large magnetic entropy in the region around and above 100 K, have been ruled out.

The above-described selections result in 14 sets of the CF parameters summarized in Table I, which do not contradict our INS, susceptibility, and specific-heat experimental data. We do not make any refinement on them to achieve ''the best fit to the experiments,'' but confine ourselves to some general

TABLE I. Crystal-field parameters describing our experimental data; the B_n^m parameters are given in units of K for $n=2$, 10^{-2} K for $n=4$, and 10^{-4} K for $n=6$.

No.	B_2^0	B_2^2	B_4^0	B_4^2	B_4^4	B_6^0	B_6^2	B_6^4	B_6^6
1	0.09	0.00	−0.05	−1.9	0.0	−0.07	1.7	−0.9	3.6
2	0.09	0.00	−0.05	1.9	0.0	−0.07	−1.7	−0.9	−3.6
3	0.14	0.00	0.00	−1.6	0.0	0.00	2.5	−0.4	1.9
4	0.14	0.00	0.00	1.6	0.0	0.00	−2.5	−0.4	−1.9
5	0.21	0.00	0.00	−1.5	0.0	0.00	2.1	−0.3	1.9
6	0.21	0.00	0.00	−1.4	0.2	0.00	2.5	0.0	2.0
7	0.21	0.00	0.00	−1.2	0.2	−0.05	2.2	0.0	3.0
8	0.21	0.00	0.00	1.2	0.2	−0.05	−2.2	0.0	−3.0
9	0.21	0.00	0.00	1.4	0.2	0.00	−2.5	0.0	−2.0
10	0.07	0.11	0.00	1.5	−0.4	0.00	−1.9	−0.4	−3.1
11	0.10	0.29	−0.05	1.9	−0.5	0.00	−1.9	−0.5	−2.7
12	0.10	−0.29	−0.05	−1.9	−0.5	0.00	1.9	−0.5	2.7
13	0.17	−0.25	−0.05	−1.6	−0.2	0.00	1.7	0.0	3.4
14	0.25	−0.18	−0.14	−1.0	1.7	−0.18	−2.5	0.0	−1.7

remarks. First we should note that the B_2^0 parameter is positive. This is in agreement with a previous assumption based on the determined magnetic structure in ErNiAl (erbium moments within the basal plane[1]) and also with a negative B_2^0 determined for the isostructural NdNiIn (Ref. 8) (the α factor has an opposite sign for Er^{3+} and Nd^{3+}) in the only CF study on an isostructural RTX compound. Unfortunately, the other B_n^m parameters given for NdNiIn (Ref. 8) can hardly be compared, because the CF has been described as hexagonal. Inspecting Table I, one can further see that the B_4^0 and B_6^0 parameters are negative or close to zero (of course, a small positive value cannot be excluded). The sign of the B_4^2 parameter is opposite to that of B_6^2, except for the set of 14 that has the smallest B_4^2 term, and the same as for B_2^2.

To investigate further the relation between the crystal charge density and the CF splitting of localized $4f$ states, we have studied the electronic structure of ErNiAl and LuNiAl. The total and site projected densities of electronic states are shown in Figs. 9 and 10, respectively. The lowest band shown in Fig. 9 is derived primarily from the Al-3s states (-9 eV$<E<-7.5$ eV). The occupied bands are derived mainly from Al-2p and Ni-3d states, which are mainly spread from -6.5 to 1.5 eV and from -3.5 to 1.0 eV, respectively, but the hybridization tail is also present far above the Fermi level. The main Er-5d(Lu-5d) bands are centered 5 eV above E_F, but the lowest of these bands dips 0.5 eV below E_F and there is a noticeable hybridized R-5dNi-3d(R-5dAl-3p) feature extending down to 6.5 eV below E_F. The Fermi level is situated in a rather flat region of the density of states (DOS) curve. The DOS in Fig. 9 indicates that, although the Ni1 and Ni2 partial DOS's provide the largest contribution near E_F, all four symmetry-inequivalent atoms are involved in the bands at or just above E_F. We note especially that Er(Lu) is not fully ionized to the 3+ state. The band features at E_F consist mainly of Er-d (Lu-d), Ni-d, and Al-p states. The energy levels of the

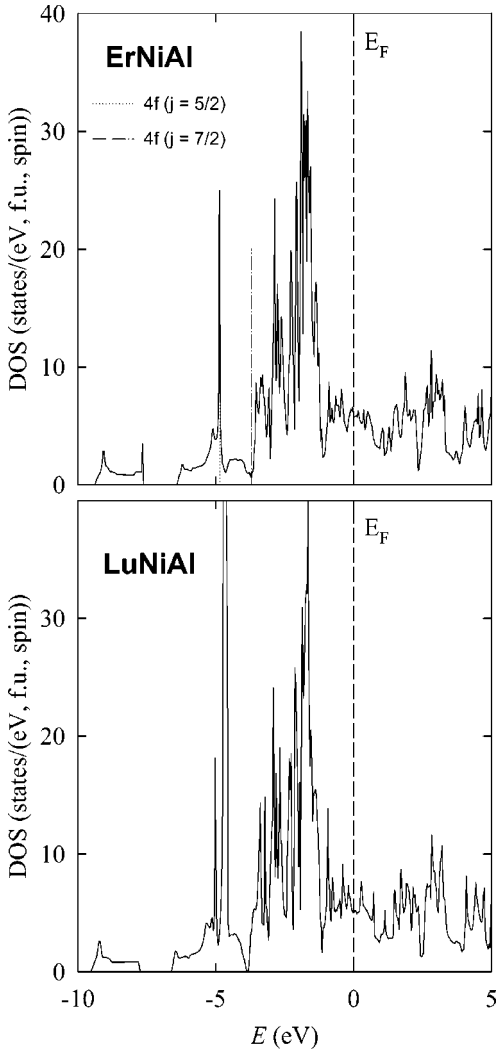

FIG. 9. Calculated scalar relativistic total nonmagnetic DOS in states per hexagonal unit cell for ErNiAl and LuNiAl. The Fermi energy is set to zero energy.

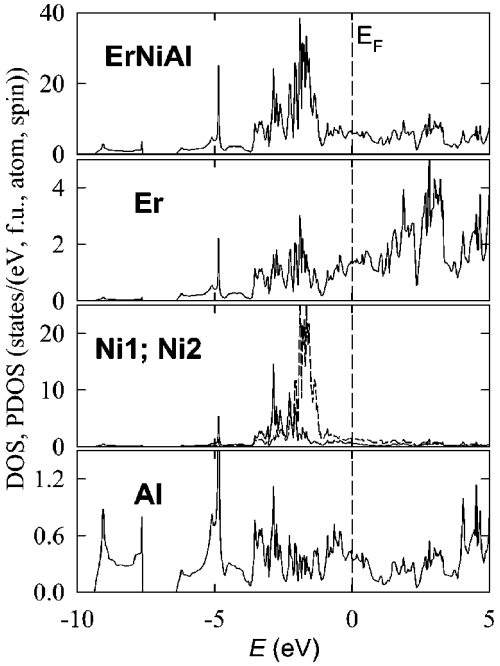

FIG. 10. Calculated scalar relativistic total and site projected nonmagnetic DOS curves in states per hexagonal unit cell of ErNiAl. The Fermi energy is set to zero energy.

$4f$ (total angular momentum quantum number $j=7/2$) and $4f$ ($j=5/2$) localized states occur at -3.71 and -4.85 eV below E_F, respectively.

In the case of $R=$Lu the $4f$ valence states are fully occupied. In our calculations the corresponding f bands were found to lie 4.7 eV below E_F, and the hybridization with the remaining valence states is very small. Thus, almost no difference in our results concerning the DOS around E_F were found, assuming the ''normal'' valence $4f$ states or ''open core'' $4f$ states.

The values of the DOS's at the Fermi level are $N(E_F)=5.8$ and 5.0 states/eV for ErNiAl and LuNiAl, respectively. In the case of LuNiAl these values correspond to $\gamma=3.9$ mJ mol^{-1} K^{-2}. The experimental specific-heat value is $\gamma=8.4$ mJ mol^{-1} K^{-2}, giving a mass enhancement factor of $\lambda=1.0$. Such a value cannot simply be interpreted as the result of the electron-phonon coupling, since the corresponding superconducting transition temperature would be $T_{SC}=12$ K using, e.g., the standard McMillan relation.[23] No sign of a superconducting transition has been observed in the resistivity data down to the 1.8 K.[24] Therefore, we suggest writing $\lambda=\lambda_{ph}+\lambda_{e-e}+\lambda_{sf}$, arguing that in addition to the contributions λ_{ph} from the electron-phonon interaction, there is also some contribution from the electron-electron interaction, which can be roughly estimated to be as large as $\lambda_{e\text{-}e}\cong 0.3$ from the analysis of the electronic specific heat for transition metals.[25] Finally an important contribution λ_{sf} should come from nickel spin-fluctuations.

Using Eqs. (3) and (4) for Er in the regular sites in ErNiAl, as described in Sec. IV, we have obtained the value $B_2^0=0.5$ K. This value is in a fair agreement with the values obtained by simultaneous analyses of various experimental data (Table I). Thus first-principles calculations provide independent checks of our searching method. To further test the reliability of our DFT-based CF calculations, we also performed non-spin-polarized LSDA calculations including spin-orbit interaction for valence electrons, spin-polarized LSDA calculations ($4f$ electrons as spin-polarized core states), and non-spin-polarized GGA calculations. The relative change of the resulting CF parameter $\delta B_2^0/B_2^0$ was found to be less than 10% in all the above-mentioned cases.

To eliminate some of the proposed B_n^m sets and obtain a more precise determination of the CF parameters, further experiments are desirable: e.g., specific-heat data in high magnetic fields applied along different crystallographic directions, magnetic susceptibility up to high temperatures (at least $\approx$500 K), or erbium Mössbauer spectroscopy could bring about rather useful information.

V. CONCLUSIONS

Several possible sets of the CF parameters have been found to describe the inelastic neutron spectroscopy, magnetic susceptibility, and specific-heat experimental data. We have fully determined the lower half of the ground-state multiplet energy-level scheme in ErNiAl. The B_2^0 crystal-field parameter is found to be positive, and the sign of some other CF parameters is tentatively concluded. Magnetic-susceptibility data show a rather weak magnetocrystalline anisotropy. Electronic structure calculations provided basic information about the bonding in ErNiAl, and confirmed the positive sign of B_2^0.

ACKNOWLEDGMENTS

We acknowledge the support from ILL technical services. The work was supported by the Grant Agency of the Czech Republic (Grant Nos. 202/98/P245 and 202/00/1602) and by the Grant Agency of Charles University (Grant No. 145/2000/B-FYZ). One of us (P.J.) acknowledges support of his stay in Japan by the Ministry of Education, Science, Sports and Culture of Japan (International Research Program: Joint Research #09044097).

*Corresponding author. Fax: +420 2 21911351. Email address: javor@mag.mff.cuni.cz

[1] P. Javorský, P. Burlet, E. Ressouche, V. Sechovský, H. Michor, and G. Lapertot, Physica B **225**, 230 (1996).

[2] P. Javorský, P. Burlet, V. Sechovský, R.R. Arons, E. Ressouche, and G. Lapertot, Physica B **234-236**, 665 (1997).

[3] G. Ehlers and H. Maletta, Z. Phys. B: Condens. Matter **101**, 317 (1996).

[4] A. Szytuła, B. Penc, M. Kolenda, J. Leciejewicz, N. Stüsser, and A. Zygmunt, J. Magn. Magn. Mater. **153**, 273 (1996).

[5] A.V. Andreev, P. Javorský, and A. Lindbaum, J. Alloys Compd. **290**, 10 (1999).

[6] P. Javorský, P. Svoboda, S. Nishigori, and M. Hofmann, Mater. Sci. Forum **324**, 705 (1999).

[7] P. Javorský, H. Nakotte, R.A. Robinson, and T.M. Kelley, J. Magn. Magn. Mater. **186**, 373 (1998).
[8] H. Fujii, T. Inoue, Y. Andoh, T. Takabatake, K. Satoh, Y. Maeno, T. Fujita, J. Sakurai, and Y. Yamaguchi, Phys. Rev. B **39**, 6840 (1989).
[9] N.C. Tuan, V. Sechovský, M. Diviš, P. Svoboda, H. Nakotte, F.R. de Boer, and N.H. Kim-Ngan, J. Appl. Phys. **73**, 5677 (1993).
[10] M.T. Hutchings, Solid State Phys. **16**, 227 (1964).
[11] U. Walter, J. Phys. Chem. Solids **45**, 401 (1984).
[12] Z. Liu, M. Richter, M. Diviš, and H. Eschrig, Phys. Rev. B **60**, 7981 (1999).
[13] M. Diviš, V. Nekvasil, and J. Kuriplach, Physica C **301**, 23 (1998).
[14] J.P. Perdew, S. Burke, and M. Ernzerhof, Phys. Rev. Lett. **77**, 3865 (1996).
[15] P. Blaha, K. Schwarz, and J. Luitz, WIEN97, Vienna University of Technology 1997 [improved and updated Unix version of the original copyrighted WIEN code by P. Blaha, K. Schwarz, P. Sorantin, and S.B. Trickey, Comput. Phys. Commun. **59**, 399 (1990)].
[16] M. Richter, J. Phys. D **31**, 1017 (1998).
[17] C. Ambosch-Draxl, P. Blaha, and K. Schwarz, J. Phys.: Condens. Matter **6**, 2347 (1994).
[18] P. Novák, Phys. Status Solidi B **198**, 729 (1996).
[19] V. Sechovský and L. Havela, in *Handbook of Magnetic Materials*, edited by K.H.J. Buschow (Elsevier, Amsterdam, 1998), and references therein.
[20] P. Javorský, P. Burlet, V. Sechovský, A.V. Andreev, J. Brown, and P. Svoboda, J. Magn. Magn. Mater. **166**, 133 (1997).
[21] C.A. Martín, J. Phys.: Condens. Matter **3**, 5967 (1991).
[22] B.R. Cooper, in *Magnetic Properties of Rare Earth Metals*, edited by R. J. Elliott (Plenum, New York, 1972), p. 44.
[23] W.L. McMillan, Phys. Rev. **167**, 331 (1968).
[24] N.C. Tuan, Ph.D. thesis, Charles University, Prague, 1992.
[25] G.S. Tripathi and S. Mohapatro, Solid State Commun. **85**, 701 (1993).